Clarifying the Copper Coordination Environment in a de Novo Designed Red Copper Protein

Karl Koebke, Leela Ruckthong, Jennifer Meagher, Emilie Mathieu, Jill Harland, Aniruddha Deb, Nicolai Lehnert, Clotilde Policar, Cédric Tard, James Penner-Hahn, et al.

Clarifying the Copper Coordination Environment in a *de Novo* Designed Red Copper Protein

Karl J. Koebke,[†] Leela Ruckthong,[†] Jennifer L. Meagher,[‡] Emilie Mathieu,[§] Jill Harland,[†] Aniruddha Deb,[†] Nicolai Lehnert,[†] Clotilde Policar,[§] Cédric Tard,[∥] James E. Penner-Hahn,[†] Jeanne A. Stuckey,[‡] and Vincent L. Pecoraro*[,†]

[†]Department of Chemistry and [‡]Life Sciences Institute, University of Michigan, Ann Arbor, Michigan 48109, United States

[§]Laboratoire des biomolécules, LBM, Département de chimie, École normale supérieure, PSL University, Sorbonne Université, CNRS, 75005 Paris, France

[∥]LCM, CNRS, Ecole Polytechnique, Université Paris-Saclay, 91128 Palaiseau Cedex, France

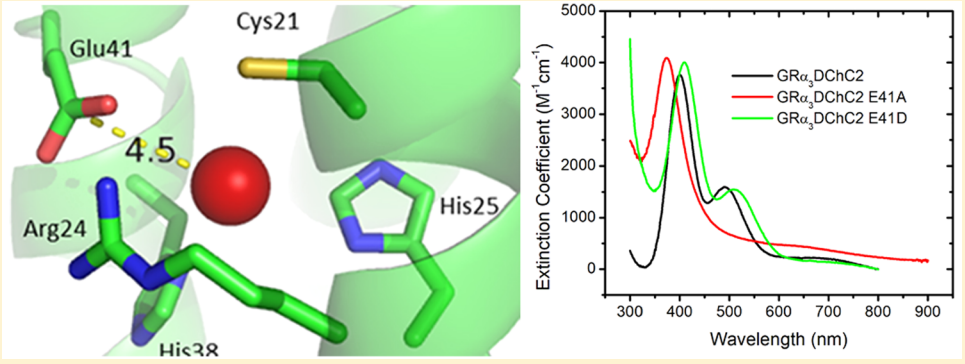

ABSTRACT: Cupredoxins are copper-dependent electron-transfer proteins that can be categorized as blue, purple, green, and red depending on the spectroscopic properties of the Cu(II) bound forms. Interestingly, despite significantly different first coordination spheres and nuclearity, all cupredoxins share a common Greek Key β-sheet fold. We have previously reported the design of a red copper protein within a completely distinct three-helical bundle protein, α_3DChC2.[1] While this design demonstrated that a β-barrel fold was not requisite to recapitulate the properties of a native cupredoxin center, the parent peptide α_3D was not sufficiently stable to allow further study through additional mutations. Here we present the design of an elongated protein GRANDα_3D (GRα_3D) with ΔG_u = −11.4 kcal/mol compared to the original design's −5.1 kcal/mol. Diffraction quality crystals were grown of GRα_3D (a first for an α_3D peptide) and solved to a resolution of 1.34 Å. Examination of this structure suggested that Glu41 might interact with the Cu in our previously reported red copper protein. The previous bis(histidine)(cysteine) site (GRα_3DChC2) was designed into this new scaffold and a series of variant constructs were made to explore this hypothesis. Mutation studies around Glu41 not only prove the proposed interaction, but also enabled tuning of the constructs' hyperfine coupling constant from 160 to 127 × 10^{-4} cm^{-1}. X-ray absorption spectroscopy analysis is consistent with these hyperfine coupling differences being the result of variant 4p mixing related to coordination geometry changes. These studies not only prove that an Glu41−Cu interaction leads to the α_3DChC2 construct's red copper protein like spectral properties, but also exemplify the exact control one can have in a *de novo* construct to tune the properties of an electron-transfer Cu site.

INTRODUCTION

Cupredoxins are copper electron-transfer proteins found within bacteria, algae, animals, and plants[2−4] that can be characterized into blue,[5−7] green,[8−11] red,[12] and binuclear purple[13−16] copper proteins depending on the spectroscopic properties of the Cu(II)-bound forms. These proteins quickly garnered the attention of the bioinorganic community due to their unique UV−vis absorption spectra with high-intensity bands at 400−450 and 550−600 nm (later assigned to σ and π ligand-to-metal charge-transfer (LMCT) bands, respectively) and unusual electron paramagnetic resonance (EPR) signals with compressed parallel hyperfine constant below 100 × 10^{-4} cm^{-1}.[1,4,17,18] The ratio between σ and π LMCT intensities is often used as a qualifier between blue/perturbed blue or type 1 copper proteins, green/purple or type 1.5 copper proteins, and red or type 2 copper proteins.[4,19,20]

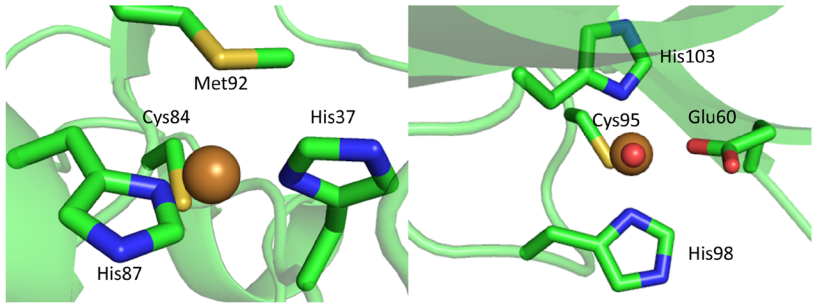

Figure 1. Pymol illustration comparing the Cu(II) binding geometries of (left) the blue copper protein poplar plastocyanin PDB 4DPB to (right) the red copper protein *Nitrosomonas europaea* nitrosocyanin PDB 1IBY.

Table 1. Amino Acid Sequences of the Peptides Discussed[a]

α_3D	MGSWAEFKQR	LAAIKTR	LQAL	GGS	
	EAELAAFEKE	IAAFESE	LQAY	KGKG	
	NPEVEALRKE	AAAIRDE	LQAYRHN		
α_3DIV	MGSWAEFKQR	LAAIKTR	**C**QAL	GGS	
	EAE**C**AAFEKE	IAAFESE	LQAY	KGKG	
	NPEVEALRKE	AAAIRDE	**C**QAYRHN		
α_3DChC2	MGSWAEFKQR	**I**AA**C**KTR	**H**QAL	GGS	
	EAELAA**H**EKE	IAAFESE	LQA**F**	KGKG	
	NPEVEALRKE	AAAIRDE	LQA**F**R**L**N	GSGA	
GRα_3D	MGSWAEFKQR	LAAIKTR	LAAIKTR	LQAL	GGS
	EAELAAFEKE	IAAFESE	IAAFESE	LQAY	KGKG
	NPEVEALRKE	AAAIRDE	AAAIRDE	LQAYRHN	GSGA
GRα_3DChC2	MGSWAEFKQR	LAAIKTR	**I**AA**C**KTR	**H**QAL	GGS
	EAELAA**H**EKE	IAAFESE	IAAFESE	LQA**F**	KGKG
	NPEVEALRKE	AAAIRDE	AAAIRDE	LQA**F**R**L**N	GSGA

[a]Mutations from the parent peptide (α3D or GRα3D) are in bold, and the heptad duplicated in the design of GRα3D is highlighted.

The prototypical cupredoxins are unequivocally blue or type 1 copper proteins, which exhibit a high intensity π LMCT (ε_π) at ~600 nm and a lower intensity σ LMCT (ε_σ) at ~450 nm with an $\varepsilon_{\sigma/\pi} < 1$.[7] Type 1.5 copper proteins instead have similarly intense σ and π LMCT peaks at 430−450 and ~570 nm, respectively, and $1 < \varepsilon_{\sigma/\pi} < 2$.[8] Finally, red or type 2 cupredoxins have very few examples, a high-intensity σ LMCT at 390 nm, lower intensity π LMCT at ~500 nm, and $\varepsilon_{\sigma/\pi} > 2$, and they are the only natural cupredoxin type with EPR hyperfine coupling above 100×10^{-4} cm^{-1}.[21]

Cupredoxin ligand sets all have a common His_2Cys primary coordination sphere, with a variable fourth ligand dependent on cupredoxin classification. This fourth ligand varies between Met and Gln for blue and green copper proteins, with little correlation between the ligand and spectroscopy, while nitrosocyanin is unique in its ligand set with a relatively short Cu(II)−Glu bond. Table S2 in the Supporting Information provides Cu(I) and Cu(II) ligand bond distances in a number of cupredoxins, and it is instructive to focus on a few examples from this list. The blue copper protein poplar plastocyanin has Cu(I)−His distances of 1.98 and 2.10 Å, a Cu(I)−Cys distance of 2.18 Å, and a relatively long Cu(I)−Met distance of 2.71 Å at pH 8. Minimal change in this structure is seen upon oxidation at pH 8 with Cu(II)−His distances of 1.91 and 2.06 Å, a Cu(II)−Cys distance of 2.07 Å, and a Cu(II)−Met distance of 2.82.[22] The green copper site within *Alcaligenes faecalis* Cu nitrite reductase has a structure similar to plastocyanin with Cu(I)−His distances of 2.06 and 2.18 Å at pH 4, a Cu(I)−Cys distance of 2.21 Å, and a Cu(I)−Met distance of 2.41 Å, and oxidized distances of 2.07 and 2.06 Å for Cu(II)−His, 2.22 Å for Cu(II)−Cys, and 2.48 Å for Cu(II)−Met.[23] The red copper site of nitrosocyanin is unique among cupredoxins, with a long Cu(I)−His at 2.36 Å at pH 7.5 as well as the more standard one at 2.01 Å, a relatively long Cu(I)−Cys of 2.26 Å, and a short Cu(I)−Glu distance of 2.03 Å. Upon oxidation, the site sees a drastic change in this long Cu−His distance with Cu(II)−His of 1.97 and 2.02 Å, similar distances for Cu(II)−Cys and Cu(II)−Glu at 2.26 and 2.09 Å, respectively, and a ligated water at 2.25 Å.[24]

Detailed spectroscopic analysis combined with structural data for red, green, and blue copper proteins has revealed that while green and blue copper proteins are closely related, red copper proteins are unique.[4,8,21,25] Comparing a series of blue and green copper proteins with the same $CuHis_2CysMet$ ligand set, we see that going from blue to green, the Cu(II)−Cys distance lengthens, while the Cu(II)−Met distance shortens. These changes are coupled with a tetragonal distortion more prevalent in green copper proteins, which increases the intensity of the σ charge transfer while decreasing that of the π charge transfer and increasing the $\varepsilon_{\sigma/\pi}$ ratio. Expanding this comparison to the red copper protein nitrosocyanin, much larger differences are found. The axial Met/Gln ligation of blue/green copper proteins is replaced by His ligation in nitrosocyanin while Glu ligation

replaces one of the equatorial His. This rearrangement of the ligand set results in a rotation of the C−S−Cu plane and allows for nitrosocyanin to bind an equatorial water not seen in other cupredoxins (Figure 1).

Metalloprotein design has proven to be a useful strategy to test the limits of our understanding of metal binding sites by mimicking those found in native proteins.[26−31] Cupredoxins have been the target of many metalloprotein design efforts due to their uniquely constrained metal binding centers and spectral properties.[4,6,7,17,32] Approaches employing protein redesign using azurin as a scaffold,[20,28,33−35] *de novo* design within three or four helical bundles,[1,36−38] and artificial metalloproteins[39] have been explored. DeGrado et al. designed a single polypeptide that formed an antiparallel 3-helix bundle called α_3D,[40,41] and this scaffold has been modified to serve as a heavy metal binding protein,[42] capable of binding Cd(II) or iron in a tetrathiolate center.[43,44] With respect to copper electron-transfer proteins, previous results from our laboratory have shown that a nitrosocyanin-like red copper center with a σ LMCT at 401 nm, π LMCT 500 nm, and $\varepsilon_{\sigma/\pi}$ = 2.2 can be designed into α_3D[40,41] using seven amino acid mutations to create α_3DChC2 (Table 1).[1] This design utilized three mutations to create a metal-binding His_2Cys core, while another four nearby mutations were meant to enclose this copper-containing region in a hydrophobic box that constrained the metal environment through steric interactions. While spectroscopic signatures confirmed that the Cu(II) form of α_3DChC2 was most accurately described as a red copper protein, X-ray absorption spectroscopy (XAS) analysis showed that the reduced construct could structurally mimic the distinct short Cu(I)−S distance common to all cupredoxins. Thus, it was hypothesized that modeling the Cu(II) form of a cupredoxin within a three-helical bundle is more challenging than the Cu(I) form.

Previous studies of the construct apo-α_3DIV, which has three residues of α_3D mutated to cysteines, revealed a solution NMR structure that was closely similar to the parent α_3D, and denaturation experiments further indicated it was a well-folded protein.[45] However, additional mutations such as those in the α_3DChC2 sequence led to proteins of markedly inferior thermodynamic stability. It was also considered that, for this reason, the α_3DChC2-designed hydrophobic box was imperfectly constraining the metal binding site, causing the red copper spectral properties. The present work was an attempt to test the above hypothesis, investigate the cause of α_3DChC2's red copper-like properties, and tune the spectral properties of this *de novo* red copper protein toward those of a blue or green copper protein in its Cu(II) form.

Previous experience with three-stranded coiled coils has shown that the stability of these complexes can be increased notably by duplicating heptads in each coil to lengthen the complex and increase the surface area of the interior hydrophobic interactions (~8 kcal/mol/heptad).[46,47] The added stability potentially gained through the added heptads would allow the new protein to tolerate additional mutations. Based upon these studies, we present the design of a more thermodynamically stable version of α_3D called GRANDα_3D (GRα_3D) as well as its crystal structure solved to a resolution of 1.34 Å, the first X-ray crystal structure determined for a member of the α_3D protein family. This crystal structure and a structure of GRα_3DChC2 predicted by the Robetta server[48−50] were used to re-examine the proposition that perturbation of the hydrophobic box might yield a red copper center for the α_3DChC2 cupredoxin mimic. Also, this construct allows one to address through mutation studies whether other residues might be consequential to the formation of the red copper center. In this context, an important surface residue (Glu41) was shown to be critical for the red copper behavior, an observation that leads to a model with a coordinated carboxylate to Cu(II) in GRα_3DChC2, which is consistent with the coordination environment found in native red copper proteins such as nitrosocyanin.

MATERIALS AND METHODS

All reagents were purchased from Sigma-Aldrich or Fisher Scientific unless otherwise specified. Cupric chloride dihydrate in crystalline form was purchased from Mallinckrodt, disodium DL-malate from TCI America, and sodium thiocyanate from Acros Organics.

Molecular Biology/Purification. In this study, either genes were purchased as gblocks from Integrated DNA Technologies before cloning into pET15B using In-Fusion cloning protocol (clontech) or, for less involved DNA changes, mutations were introduced to an existing plasmid by reverse PCR before using the In-Fusion protocol to re-cyclize the resulting mutated plasmid. All completed plasmids were transformed into BL21 (DE3) *Escherichia coli* and the sequences of the cloned genes confirmed by Sanger Sequencing at the University of Michigan DNA Sequencing Core.

Constructs were expressed using an overnight autoinduction protocol with 12 g of tryptone, 24 g of yeast extract, 2.3 g of potassium phosphate monobasic, 12 g of potassium phosphate dibasic, 0.083 g of lactose, 0.4 g of glucose, 1.66 mL of 50% glycerol, and 100 mg of ampicillin per liter of growth media. Starter cultures of LB with 100 mg/L ampicillin were inoculated with frozen cell stock and incubated at 37 °C with 250 rpm shaking for 5−7 h. Each liter of autoinduction media was then inoculated using 10 mL of this starter culture and incubated at 25 °C and 250 rpm overnight in UltraYield flasks. After 14−18 h, the cells were harvested by centrifugation and lysed by a microfluidizer, while peptide was purified using previously published methods.[51] Final OD_{600}'s of these autoinduction cultures varied between 6 and 16, with purified peptide yields of 30−200 mg/L.

Spectroscopy. Electronic absorption data were collected on a Cary 100 UV−vis spectrometer. Electron paramagnetic resonance spectra were collected using a Bruker EMXE 200 EPR instrument. Circular dichroism (CD) measurements and guandinium titration data were taken using a Jasco J-1500 CD spectropolarimeter with an ATS-530 automatic titrator. Mass and purity of peptide solutions were determined by Micromass LCT TOF MS.

Magnetic Circular Dichroism. First, 1 mM Cu(II) acetate was added to a 1.5 mM peptide solution in 50 mM HEPES buffer at pH 7.5 with 50% glycerol (added as a glassing agent) immediately before being injected between two quartz plate windows housed in a custom-made MCD sample holder. The samples were frozen in liquid nitrogen to produce a glass.

The MCD setup employs an Oxford SM4000 cryostat and a Jasco J-815 CD spectrometer. The SM4000 cryostat consists of a liquid helium-cooled superconducting magnet providing horizontal magnetic fields of 0−7 T. The J-815 spectrometer uses a gaseous nitrogen-cooled xenon lamp and a detector system consisting of two interchangeable photomultiplier tubes in the UV−vis and near-infrared (NIR) ranges. The samples were loaded into a 1.5−300 K variable-temperature insert (VTI), which offers optical access to the sample via four optical windows made from Suprasil B quartz. The MCD spectra were measured in $[\theta]$ = mdeg and manually converted to $\Delta\varepsilon$ (M^{-1} cm^{-1} T^{-1}) using the conversion factor $\Delta\varepsilon = \theta/(32980 \times c \times d \times B)$, where c is the concentration, B is the magnetic field, and d is the path length.[52] The product $c \times d$ can be substituted by $A_{MCD}/\varepsilon_{UV-vis}$, where A is the absorbance of the sample measured by the CD spectrometer. Complete spectra were recorded at different temperatures (2, 5, and 10 K) and magnetic fields (0−7 T). Gaussian deconvolution of the spectra was performed using the program PeakFit.

X-ray Crystallography. Crystals of GRα_3D (40 mg/mL) with 15 mM $Zn(OAc)_2$ and 10 mM tris(hydroxymethyl)aminomethane (TRIS) buffer at pH 8.5 were grown by sitting drop vapor diffusion against a well solution of 2.1 M disodium DL-malate at pH 7.0, containing 200 mM sodium thiosulfate as an additive at 20 °C. Crystals were cryoprotected in mother liquor containing 10% ethylene glycol and then supercooled in liquid N_2 for data collection.

Crystal diffraction data were collected at the Advanced Photon Source of the Argonne National Laboratory on the LS-CAT Beamline 21-ID-G, equipped with a Mar 300 CCD detector. The data were collected with a 1° oscillation and then processed and scaled with HKL2000.[53] The structure was solved by the single anomalous dispersion technique using the AutoSol[54] program in Phenix,[55] giving a partial model containing amino acids 4−28 of helix A and 38−85 of helices B and C. This partial model was verified by using it as a search model for auto MolRep[56] in the CCP4 suite of programs.[57−59] The solution from molecular replacement was then carried through to refinement. The electron difference density map ($F_o - F_c$) contoured at 3σ shows a Zn(II) binding site on the exterior of the three-helix bundle at Glu6. A second Zn(II) is present as a part of the complex polyanion $Zn(SCN)_4^{2-}$. While $Zn(SCN)_4^{2-}$ is commonly observed in solutions in which Zn(II) is in the presence of excess NaSCN, we were unable to find another instance of this polyanion within a protein structure deposited in the Protein Data Bank. Missing residues from the N and C termini as well as the loop between helices A and B were built in manually using the electron density map. The N-terminal methionine could not be modeled into the crystal structure; however, the missing Met is corroborated by mass spectrometry, has been seen in previous α_3D expressions,[60] and can be explained by methionine aminotransferase's relative activity for an N-terminal Met followed by Gly.[61] The structure underwent iterative rounds of electron density fitting and refining in Coot[62] and Buster 2.10.2[63] programs, respectively. The MolProbity[64] program was used to verify the validity of the final model (Table 2). All residues are present in the allowed regions of the Ramanchandran plot.

X-ray Absorption Spectroscopy. Cu(I) samples were prepared as follows. Solutions were made with a final concentration of 1 mM tetrakis(acetonitrile)Cu(I)hexafluorophosphate in 1.5 mM peptide solution in 50 mM HEPES buffer at pH 7.5 with 50% glycerol (added as a glassing agent) in the glovebox maintained in anaerobic conditions. Sample solutions were then loaded into a sample cell and frozen in liquid nitrogen; 0.5 mM excess apo peptide was included to ensure the free Cu^I concentration was minimal (<0.01%).

Cu(II) samples were prepared with final concentrations of 1 mM Cu(II)acetate and 1.5 mM peptide in 50 mM HEPES buffer at pH 7.5 in aerobic conditions. Samples were then lyophilized before being transferred to sample cells. During collection, the Cu edge energy and 1s→4p transition of Cu(I)peptide were monitored. We estimate that no more than 10% of the sample was photoreduced by the final scan included in fitting.

Measurements were carried out at Stanford Synchrotron Radiation Lightsource (SSRL) beamline 7-3 or 9-3 with a Si(220) double-crystal monochromator and a flat Rh-coated harmonic rejection mirror. Samples were maintained below 10 K with an Oxford Instruments liquid helium cryostat. Data were measured as fluorescence excitation spectra using a 30- or 100-element Ge detector array (for beamlines 7-3 or 9-3, respectively) normalized to incident intensity measured with a N_2-filled ion chamber. Data were measured with steps of 0.25 eV in the XANES region (1 s integration time) and 0.05 $Å^{-1}$ in the EXAFS region to k = 13.5 $Å^{-1}$ (1−20 s integration, k^3 weighted). Energies were calibrated by assigning the lowest energy inflection point of a copper metal foil as 8980.3 eV. The threshold energy, E0, was defined as 8991 based on fits of model compounds; this was used to convert data to k-space, and the background was removed using a three-region cubic spline. EXAFS data were analyzed using EXAFSPAK[66] and FEFF 9.0.[67] XANES data were normalized using MBACK.[68]

Single- and multiple-scattering fitting of EXAFS data were performed using EXAFSPAK[66] with *ab initio* amplitude and phase parameters calculated using FEFF 9.0.[67] An initial model of Cu−imidazole coordination was built based on the averaged bond distances determined by single-scattering fitting of EXAFS data.

Table 2. Crystallography Data Collection and Refinement Statistics for GRα_3D

Data Collection	
PDB ID	6DS9
space group	*P*3
wavelength (Å)	0.97856
resolution (Å)[a]	1.34 (1.34−1.36)
R_{sym} (%)[b]	3.3 (32.4)
$\langle I/\sigma I \rangle$[c]	20 (2)
completeness (%)[d]	98.8 (82.1)
redundancy	5.5 (3.6)
Refinement	
resolution (Å)	1.34 (9.23−1.34)
R-factor (%)[e]	18
R_{free} (%)[f]	18.6
no. protein atoms	720
no. metal atoms	2 Zn at 0.33 occupancy
no. water molecules	43
no. unique reflections	18 658
rmsd[g]	
bonds (Å)	0.01
angles (deg)	0.97
MolProbity score[64]	1.06
Clash score[65]	1.87

[a]Statistics for highest resolution bin of reflections in parentheses. [b]$R_{sym} = \sum_h \sum_j |I_{hj} - \langle I_h \rangle| / \sum_h \sum_j I_{hj}$, where I_{hj} is the intensity of observation j of reflection h and $\langle I_h \rangle$ is the mean intensity for multiply recorded reflections. [c]Intensity signal-to-noise ratio. [d]Completeness of the unique diffraction data. [e]*R*-factor = $\sum_h ||F_o| - |F_c|| / \sum_h |F_o|$, where F_o and F_c are the observed and calculated structure factor amplitudes for reflection h. [f]R_{free} is calculated against a 10% random sampling of the reflections that were removed before structure refinement. [g]Root mean square deviation of bond lengths and bond angles.

Electrochemical Potential Determination. Cyclic voltammetry measurements were obtained on a Metrohm AUTOLAB potentiostat (PGSTAT 302N). The electrochemical apparatus contained a gold disk working electrode (0.002 cm^2), a platinum wire counter electrode, and an aqueous saturated calomel electrode (SCE) as the reference electrode (0.241 V + SCE = normal hydrogen electrode). The gold electrode surface was carefully polished and sonicated before being conditioned in an electrochemical cell which contained 0.5 M H_2SO_4 by scanning 20 times from −300 to +1500 mV (vs SCE) at 200 mV/s, and then in a cell which contained 0.1 M phosphate buffer (pH 7.4) and 0.1 M Na_2SO_4 by scanning four times from −300 to +600 mV (vs SCE) at 100 mV/s, until the cyclic voltammograms overlaid well enough to indicate a homogeneous surface. The Cu−peptide solutions were prepared with 15 mM peptide, 10 mM $CuSO_4$, and 50 mM ascorbate in a 0.1 M phosphate buffer solution (pH 7.4). After each electrode had been polished and conditioned, 20−50 μL of a 0.5 mM peptide solution was adsorbed on the gold electrode surface for 2 h. Cyclic voltammograms were collected under anaerobic conditions (argon) in a cell which contained 0.1 M phosphate buffer (pH 7.4) and 0.1 M Na_2SO_4 at varying scan rates and at room temperature (~21 °C).

Model Illustration. Models of GRα_3DChC2 were created using SCWRL4[69] to mutate the appropriate amino acids within the GRα_3D sequence and repack the entire structure while keeping the backbone scaffold fixed. Putative positions for the bound Cu(II) were then explored using Pymol visualization.

RESULTS

GRα_3D Structure. The original α_3D and α_3DIV have an α-helical region ~27 Å in length, while that in GRα_3D is ~34 Å. Secondary structure assignment by the VADAR Web server also indicates a longer continuous region of α-helicity in GRα_3D (84/93 or 90%) compared to α_3D and α_3DIV (56/73 or 76%), beyond that expected from the duplication of a single heptad.[70] This unanticipated increase in helical content stems from a lower number of amino acids being in random coil form for each turn between helices. α_3D's A and B helices are connected by an eight-residue coil region from Leu21 to Leu28, while B and C helices are connected by five residues from Ala44 to Lys48. The comparable regions in GRα_3D are instead four residues (Leu28 to Ser31) and two residues in length (Gly63 to Asn64) (Figure 2).

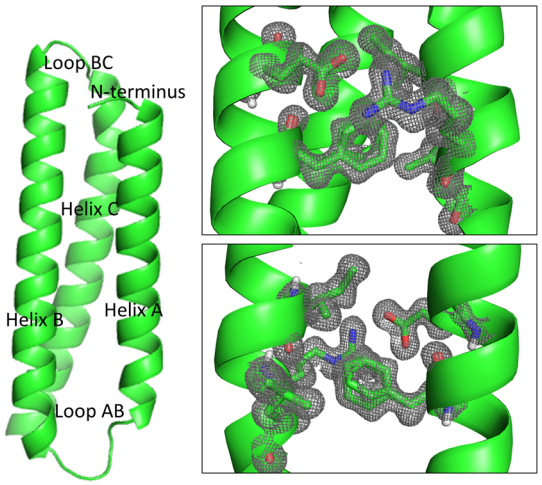

Figure 2. (Left) Pymol cartoon representation of GRα_3D showing overall secondary structure. (Right) $2F_o - F_c$ electron density map (gray grid) contoured at 1σ, overlaid onto the stick representation of amino acids Ile21, Arg24, Leu25, Phe38, and Glu41, which were mutated during the course of this study.

Previously our group has reported that incorporating a Cys_3 site into α_3D to make α_3DIV improved the packing between several hydrophobic layers.[45] Comparing the structures of GRα_3D and α_3D, we find a similar effect, particularly when examining the repeated heptad used in GRα_3D's design. (Table S3) The hydrophobic layers of GRα_3D defined by Phe7, Leu11, and Ile14 of helix A have triangular areas reduced by 8.63, 5.17, and 5.53 Å^2, respectively, when compared to that of α_3D. Comparing the void volume and packing density using the Web server ProteinVolume 1.3[71] also exhibits this difference between the two structures, with packing densities of 0.781 and 0.766 for GRα_3D and α_3D, respectively. GRα_3D's increased packing density is largely caused by a reduced distance between helix A and its two partner helices, while the distance between helices B and C remains similar between the two constructs (Figure S1).

Folding Free Energy. The increased α-helical region of GRα_3D was hypothesized to lead to a concomitant increase in thermodynamic stability compared to that of α_3D.[41] Guanidinium denaturation titrations were used to determine folding free energy for GRα_3D at pH 5 and 8.5 as well as for GRα_3DChC2 and GRα_3DChC2 E41Q at pH 8.5 to investigate this possibility (Table 3). We were previously unable to calculate the stability difference associated with mutation of α_3D to α_3DChC2 due to the latter's low folding free energy. Comparison of GRα_3D to

Table 3. Circular Dichroism Properties for Several GRα_3D Derivatives Compared to Literature Values for α_3D[41a]

	m (kcal mol^{-1} M^{-1})	C_m (M)	ΔG_u (kcal mol^{-1})
α_3D, pH 5	2.4	2.8	5.1
GRα_3D, pH 5	2.79(0.11)	4.1(0.2)	11.4(0.1)
GRα_3D, pH 8.5	3.11(0.23)	3.9(0.2)	12.0(0.3)
GRα_3DChC2, pH 8.5	2.04(0.31)	1.9(0.2)	3.9(0.7)
GRα_3DChC2 E41Q, pH 8.5	2.48(0.16)	1.7(0.2)	4.1(0.2)

[a]Parameters for GRα_3D were calculated based on a two-state model of denaturation.[73]

GRα_3DChC2 gives a destabilizing effect of ~8 kcal/mol at pH 8.5 (Table 3) for incorporation of the ChC2 metal binding site, as compared to destabilizations of 3.7, 3.8, and 1.9 kcal/mol for the other three cupredoxin models reported in previous work.[1] This destabilization of ChC2 incorporation is related not only to a decrease in C_m but also to the slope m, which is linked to unfolding cooperativity. This change is likely due to the disruptive effect of mutating two core hydrophobic residues to His residues into the relatively tight confines of the hydrophobic core.[72] E41Q mutation to this construct, however, has no destabilization effect, leaving us confident that disruption of the E41−R24 salt bridge of GRα_3DChC2 does not have a large effect on structural stability.

Cu(II) Spectroscopy and Electrochemistry. Electronic absorption and EPR spectra were collected for Cu(II) adducts of GRα_3DChC2 and its E41Q, E41D, R24M, and R24A variants to investigate a previously reported hypothesis that the red copper-like spectroscopic properties of α_3DChC2 are due to that construct's low free energy of folding as well as the newly presented possibility that the aforementioned spectroscopic properties are due to an unexpected interaction with residue Glu41. UV−visible spectroscopy of the above constructs were followed for up to 2 days at 25 °C to compare the half-life of the peptide bound Cu(II) signal. Constructs which exhibited interesting spectroscopic differences were chosen for electrochemical analysis. Standard potentials were measured using Au-grafted constructs of GRα_3DChC2 and its E41Q, E41D, and E41A variants with GSGC C-terminal ends rather than the standard GSGA included to improve peptide yields (Table 4).

MCD spectra were collected on GRα_3DChC2 and its E41D variant. These were combined with those constructs' electronic absorption spectra to deconvolute the energies of the observed optical transitions. The correlated fits of the UV−vis absorption versus MCD data for the two proteins are shown in Figure S6. The energies of these bands are provided in Table 5, along with those previously reported for nitrosocyanin (derived from the low-temperature MCD data) for comparison.[21] Please note that the electronic transitions in both of our constructs show an unusual shift to higher energy between the room-temperature UV−vis and liquid He temperature MCD data, as evident from the fits in Figure S6. This effect results from the freezing of the protein sample, required for the low-temperature experiments. The CD spectrometer records a low-resolution absorption spectrum at the same time that the MCD spectrum is measured, and in this spectrum, the intense band 1 (σ CT) is shifted by +800 cm^{-1} in the absorption spectrum of GRα_3DChC2 between room temperature and liquid He temperature, in agreement with the deviations in band energies observed between the UV−vis and MCD data. Band assignments of GRα_3DChC2 and its E41D variant in Table 5 are based on the comparison to the MCD

Table 4. Spectroscopic Parameters of All Proteins Presented in This Work as Well as Cu(II) Signal Lifetimes

construct	σ LMCT λ_{max} (ε)	π LMCT λ_{max} (ε)	$\varepsilon_\sigma/\varepsilon_\pi$	g (x, y, z)	$A_\parallel$ ($\times 10^{-4}$ cm^{-1})	half-life of Cu(II) signal	E^0 (mV vs NHE)
α_3DChC2	401 nm (4430)	499 nm (2020)	2.20	2.032, 2.027, 2.207	136	~8 h	+462 ± 14
GRα_3DChC2	400 nm (3760)	490 nm (1600)	2.33	2.032, 2.032, 2.203	142	~8 h	+530
GRα_3DChC2 R24A	399 nm (2520)	490 nm (1150)	2.22	2.034, 2.034, 2.209	142	~8 h	–
GRα_3DChC2 R24M	399 nm (3480)	493 nm (1450)	2.39	2.026, 2.028, 2.198	138	~8 h	–
GRα_3DChC2 E41Q	377 nm (5120)	490 nm (970)	5.27	2.029, 2.020, 2.212	154	~1 h	+510 ± 10
GRα_3DChC2 E41A	373 nm (4090)	490 nm (720)	5.68	2.052, 2.020, 2.223	160	~20 min	+510 ± 10
GRα_3DChC2 E41D	410 nm (4000)	510 nm (1550)	2.59	2.034, 2.033, 2.211	127	~8 h	+480
nitrosocyanin[12,21]	390 nm (7000)	490 nm (2200)	3.18	2.036, 2.059, 2.245	142	N/A	+85

Table 5. Deconvolution of the Low-Temperature MCD Spectra of GRα_3DChC2 and Its E41D variant, and Comparison to Nitrosocyanin

construct	band 1 (cm^{-1}) σ CT	band 2 (cm^{-1}) π CT	band 3 (cm^{-1}) d_{xy}	band 4 (cm^{-1}) d_{z^2}	band 5 (cm^{-1}) d_{yz}
GRα_3DChC2	27 173	21 345	17 825	15 432	13 800
GRα_3DChC2 E41D	24 570	20 283	16 583	13 245	–
nitrosocyanin[21]	25 550	20 350	17 500	15 000	12 900

spectrum of nitrosocyanin and the published assignments. Overall, the MCD spectra of GRα_3DChC2 and its E41D variant show very close agreement to those obtained for nitrosocyanin, demonstrating that our constructs provide overall similar copper binding sites with similar ligand fields and d-orbital energies compared to the red copper protein.

X-ray Absorption Spectroscopy. We prepared the Cu(I/II) complexes of GRα_3DChC2, GRα_3DChC2 E41A, GRα_3DChC2 E41Q, and GRα_3DChC2 E41D and subjected these to XAS in order to gain insight into the structural factors affecting the changes in spectroscopy seen between GRα_3DChC2 variants. XANES analysis of the 1s→4p transition of Cu(I) can act as a useful diagnostic of coordination number, with higher peak intensities being indicative of lower coordination number.[74] When compared in this way, the peak intensities for Cu(I)α_3DChC2 (Figure S4), Cu(I)GRα_3DChC2, Cu(I)-GRα_3DChC2 E41Q, and Cu(I)GRα_3DChC2 E41D all indicate a 2- to 3-coordinate species. EXAFS analysis of these adducts all exhibit outer-shell scattering suggestive of histidine coordination (Figure S2). Our analysis favors a model of Cu(I)His_1S_1 due to a combination of the intensity of the 1s→4p transition, the distance of the Cu−S bond in all constructs being closer to a 2-coordinate red copper protein from literature than the 3-coordinate nitrosocyanin, and the increased Debye−Waller factor of the nitrogen ligand when two His are included in the fit (Table 6 and Supporting Information). None of these indicators is definitive, so it is difficult to differentiate between the two models based on EXAFS alone. This ambiguity, however, is not a major concern, as both models give similar distances for the Cu−S and Cu−N bonds.

Analysis of the 1s→3d transition of Cu(II) can be used to indicate geometric differences between samples, as the intensity of this peak is linked to 4p mixing within this transition.[76,77] Comparing Cu(II)GRα_3DChC2 and its E41Q, E41A, and E41D variants, we find that E41D has the greatest peak area, followed by GRα_3DChC2, E41Q, and E41A in order of decreasing peak area (Figure S5). EXAFS analysis of these adducts exhibited long-distance scatterers similar to those seen in Cu(I) EXAFS (Figure S3), indicative of histidine coordination. Based on this as well as the interpretation of UV−vis and EPR spectroscopy

Table 6. Cu(I) EXAFS Fitting Parameters

		Cu−S		Cu−N	
construct	model	R (Å)	σ^2 ($\times 10^{-3}$ Å^2)	R (Å)	σ^2 ($\times 10^{-3}$ Å^2)
α_3DChC2	$CuHis_1S$	2.19	3.5	1.92	6.1
	$CuHis_2S$	2.18	4.4	1.93	12.5
GRα_3DChC2	$CuHis_1S$	2.17	5.1	1.92	8.9
	$CuHis_2S$	2.17	5.8	1.93	14.1
E41Q	$CuHis_1S$	2.18	5.9	1.94	8.2
	$CuHis_2S$	2.17	6.8	1.95	12.9
E41A	$CuHis_1S$	2.16	4.0	1.93	9.2
	$CuHis_2S$	2.16	4.3	1.95	16.2
E41D	$CuHis_1S$	2.17	2.8	1.89	7.0
	$CuHis_2S$	2.17	3.7	1.90	11.8
nitrosocyanin[21]	$Cu(N/O)_2S$	2.30	3.2	1.96	4.0
Sco C49A[75]	$CuHis_1S$	2.12	5	1.88	5

Table 7. Cu(II) EXAFS Fitting Parameters

		Cu−S		Cu−N		Cu−O	
construct	model	R (Å)	σ^2 ($\times 10^{-3}$ Å^2)	R (Å)	σ^2 ($\times 10^{-3}$ Å^2)	R (Å)	σ^2 ($\times 10^{-3}$ Å^2)
α_3DChC2	$CuHis_2S_1O_1$	2.18	5.6	1.94	6.0	2.07	1.6
GRα_3DChC2	$CuHis_2S_1O_1$	2.23	10.6	1.97	3.3	1.96	7.7
E41Q	$CuHis_2S_1O_1$	2.19	8.3	1.94	5.7	2.06	8.3
E41A	$CuHis_2S_1O_1$	2.18	8.6	1.94	7.2	2.07	6.9
E41D	$CuHis_2S_1O_1$	2.20	5.6	1.93	9.0	2.03	4.7
nitrosocyanin[21]	$Cu(N/O)_3S_1$	2.30	3.2	1.96	5.8	–	–

(*vide infra*), the data for all presented constructs were fit with $Cu(II)His_2S_1O_1$ as the model (Table 7).

DISCUSSION

Previously reported work to design a cupredoxin-like binding site within α_3D culminated in Cuα_3DChC2 with Cu(II) spectroscopic properties like those of nitrosocyanin, a red copper protein (Table 4). It was suggested that this construct's red copper-like properties rather than blue or green were due to the apo peptide's low free energy of folding. The concept of the blue copper metal binding site being in a constrained state is well established,[14,78] and the decreased folding stability of α_3DChC2, established by examination of guanidinium denaturation curves (Figure 3), suggests that the metal binding site may not be in

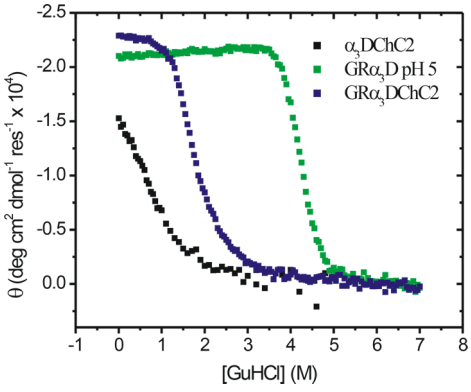

Figure 3. Guanidinium titration data for α_3DChC2, GRα_3D, and GRα_3DChC2. Sample solutions contained 10 mM Na/K phosphate buffer and 10 μM peptide, and were pH adjusted to 8.5 unless otherwise stated. Titrant solutions were identical to sample solutions with the addition of 7.5−7.8 M guanidinium hydrochloride using a saturated stock solution.

such a well-structured state. We set out to design a more stable form of the scaffold peptide α_3D to investigate whether improved thermodynamic stability of the apo peptide would shift the spectroscopic properties of Cu(II)α_3DChC2 from those of a red copper protein to green or blue.

GRα_3D is the first instance of adapting the strategy of duplicating heptads from three-stranded coiled coils to a single-stranded tri-helical bundle. The amino acid sequence of α_3D as compared to GRα_3D (Table 1) illustrates the general strategy taken for GRα_3D's design. The original α_3D required several rounds of redesign within its loop regions to create a primary sequence which folded into a single tertiary structure.[40,41] GRα_3D's design strategy was to increase the length of the α-helical region by duplicating the central heptad shown in Table 1. This design was intended to leave the loop regions unperturbed and lead to an α_3D-like single folded state with a longer α-helical bundle region and, thus, more thermodynamic stability.

Comparing the NMR structures of α_3D[41] and α_3DIV[45] to the crystal structure of GRα_3D (Figure 2), the α-helical region of GRα_3D is roughly 25% longer. GRα_3D is also notably more stable than its parent peptide, with a Gibbs free energy of unfolding more than double that of α_3D (Table 3). It is interesting to note that this improved stability is largely caused by an increase in C_m (from 2.8 to 4.1 M) but that there is also a small increase in m (from 2.4 to 2.8 kcal mol^{-1} M^{-1}) which indicates a more cooperative unfolding event. This increase in cooperativity of unfolding may be related to decreased length of the loop regions which connect α-helical portions of GRα_3D as compared to α_3D, which leads to a structure that is 90% α-helix. Thus, we have successfully created a longer, more stable version of the α_3D scaffold, which we call GRα_3D. This was the first member of the α_3D family to form diffraction-quality crystals successfully. Our laboratory has previously used the strategy of increasing α-helical length in three-stranded coiled coil constructs to, at least empirically, improve the success rate of crystallization, and this seems to have proven true of three-helical bundle designs as well.[79]

The metal binding site of α_3DChC2, including the enclosing hydrophobic box, was constructed within GRα_3D to investigate if the increased stability of apo GRα_3D could be translated to Cu(II)GRα_3DChC2 and test its effect on spectroscopic properties. Guanidinium titrations of the apo peptides (Figure 3) confirm that GRα_3DChC2 is well folded in solution with a clear two-state model of denaturation, unlike α_3DChC2. Though α_3DChC2's low Gibbs free energy of unfolding makes more-detailed comparisons impossible, the difference between GRα_3DChC2 and α_3DChC2 in apo peptide stability is clear (Figure 3). Cu(II)GRα_3DChC2, however, has spectroscopic properties very similar to those of Cu(II)α_3DChC2 regardless of this increased peptide stability (Table 4), proving that the nitrosocyanin-like properties of Cu(II)α_3DChC2 are not caused by that peptide's low free energy of unfolding. MCD deconvolution of the electronic absorption spectra allowed us to compare the d-d electronic transitions of Cu(II)GRα_3D-ChC2 to those of native nitrosocyanin, where previously we had only compared the energy of Cys σ and π LMCT bands using absorption spectroscopy. Table 5 shows remarkable similarities in the energies of all observed transitions, reconfirming our assignment of the Cys σ and π LMCT bands observed in electronic absorption spectra and the success of Cu(II)GRα_3D-ChC2 as a spectroscopic model of nitrosocyanin. Interestingly, while Cu(II)GRα_3DChC2 falls well within the spectroscopic parameters of a red copper protein, there are some notable structural and spectroscopic differences between it and Cu(II)-α_3DChC2. While, for the purposes of this study, Cu(II)GRα_3D-ChC2 can be used to probe the factors which enable a red copper *de novo* cupredoxin regardless of these differences, they

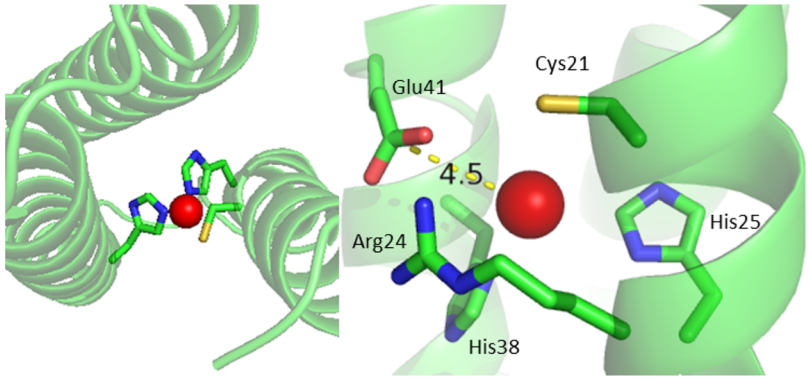

Figure 4. Pymol illustrations showing the expected position of the metal binding site of GRα_3DChC2 as predicted by SCWRL4[66] (left) and the expected Glu41−Cu distance if Cu(II) were bound in such a position.

may warrant further investigation in the future to determine their cause for future study of GRα_3D versions of metal binding sites originally designed within α_3D. We then sought to explore further the causes of Cu(II)GRα_3DChC2's red copper-like spectroscopic properties using site-directed mutagenesis—a strategy only made possible by the improved stability of GRα_3DChC2 as compared to α_3DChC2.

Modeling the Cu(II) binding site in GRα_3DChC2 by using the X-ray structure of GRα_3D with Pymol (Figure 4) brought the assigned position of the bound Cu(II) into question. Sequence analysis shows that the metal binding site in GRα_3DChC2 is formed using only two of the available α-helices, instead of all three. Therefore, the bound Cu(II) is likely positioned dissymmetrically with respect to the helical axis and toward the helical interface. This new model contrasts with a symmetrically disposed copper situated within the hydrophobic interior, as was previously postulated. This new shifted position would place the bound Cu(II) within ~5 Å of a nearby glutamate (Glu41) designed into GRα_3D as part of a salt bridge interaction (Figure 4). Given GRα_3DChC2's nitrosocyanin-like spectral properties and native nitrosocyanin's CysHis$_2$Glu Cu(II) binding motif, the possibility of inner-sphere coordination of this carboxylate warranted further investigation.

E41Q and E41A variants of GRα_3DChC2 were created to test the hypothesis that E41 directly binds Cu(II). Examination of electronic absorption spectra of Cu(II)GRα_3DChC2 E41A and Cu(II)GRα_3DChC2 E41Q compared to that of the parent exemplify the importance of this E41−Cu(II) interaction. Both mutants exhibit decreased intensity π LMCT, a higher intensity σ LMCT (blue-shifted to ~375 nm from the parent construct's 400 nm), a $\varepsilon_{\sigma/\pi}$ ratio of 5.3 or 5.7, respectively (Figure 5), somewhat rhombic EPR signals, and expanded hyperfine coupling constants (Table 4). All of these spectral changes exemplify the importance of E41. This, however, could be caused by the loss of a salt bridge between E41 and R24, leading to increased water accessibility to the bound metal ion rather than the disruption of a E41−Cu interaction. Cu(II)GRα_3DChC2 R24A and Cu(II)GRα_3DChC2 R24 M constructs, however, exhibit little difference in the UV−visible absorption and EPR properties of the bound Cu(II), which is convincing evidence that E41 is indeed bound to Cu(II), as R24A and R24 M mutations should disrupt the E41−R24 salt bridge and increase water access in a similar way as E41A or E41Q mutations. Once the E41−Cu interaction had been established, an E41D variant was created to test the effect of shortening this amino acid by a single methyl group. Interestingly, this was the

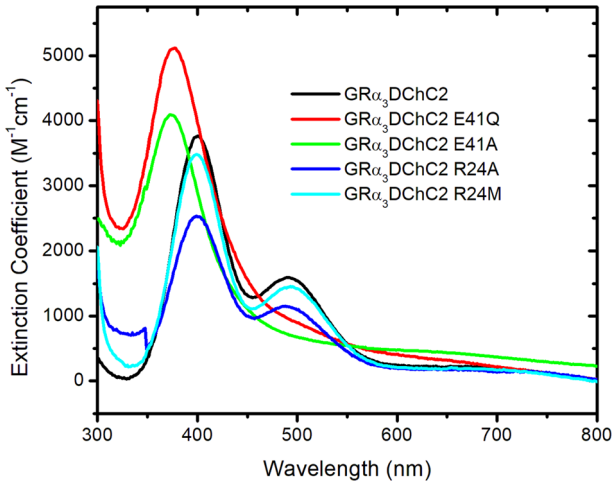

Figure 5. Extinction coefficient spectra of several GRα_3DChC2 variants to show the effect of mutations around the E41−R24 salt bridge. Solutions contained 75 μM peptide and 50 μM Cu(II) in 50 mM HEPES adjusted to pH 7.5 before the addition of Cu(II).

only E41 variant in which the hyperfine coupling constant compressed (to 127×10^{-4} from 136×10^{-4} cm^{-1}) rather than expanded, but it maintained very similar UV−vis characteristics, with σ and π LMCT peaks red-shifted by 10 and 20 nm (600 and 800 cm^{-1}) and an increased intensity ratio of 2.6 (Table 4). Further inspecting the differences between Cu(II)GRα_3DChC2 and Cu(II)GRα_3DChC2 E41D via deconvolution of MCD spectra (Table 5), we find that the four bands assigned to the Cys→Cu(II) CT and d-d transitions of Cu(II) and apparent in both constructs shift ~1000 cm^{-1} to lower energy in tandem going from the parent construct to the E41D variant, consistent with an increase in the energy of the electronic ground state, which would decrease the transition energy for all visible bands.[4]

Combining electronic absorption, EPR, and X-ray absorption spectra of Cu(II) adducts of GRα_3DChC2, GRα_3DChC2 E41Q, GRα_3DChC2 E41A, and GRα_3DChC2 E41D, we can consider the structural and electronic effects of E41 variants on the bound Cu(II). The changes from axial EPR spectra with $g_\parallel > g_\perp > 2$ seen in Cu(II)GRα_3DChC2 and Cu(II)GRα_3DChC2 E41D to the more rhombic signals of Cu(II)GRα_3DChC2 E41Q and Cu(II)GRα_3DChC2 E41A,[80,81] as well as the trend in 1s→3d transition intensity in Cu(II) XAS, are consistent with E41Q and E41A mutations causing a distortion from more tetragonal geometries of the parent and E41D variant. This distortion in the binding site geometry also helps to explain the apparently

contradictory trends seen in Cu−S distance measured by XAS and hyperfine coupling constant measured by EPR. While the hyperfine coupling constant is often used as a measure of Cu−S covalency within cupredoxins, other factors such as 4p mixing into 3d can also cause hyperfine coupling constant depression.[82,83] This orbital mixing was one of the reasons behind an early geometry assignment of native blue copper proteins as tetrahedral before the crystal structure was available and has more recently been implicated as the cause of compressed hyperfine within type zero copper proteins which contain no Cu−S bond but nevertheless exhibit compressed hyperfine.[84−89] A similar effect would explain the trend of hyperfine coupling constants seen within our *de novo* proteins, in which those with the greatest degree of 4p mixing as determined by XAS also have the most compressed hyperfine coupling. Interestingly, the series of constructs we have presented seems to be consistent with hyperfine coupling compression mostly due to geometry changes, as evidenced by differences in $\varepsilon_{\sigma/\pi}$ ratio and 1s→3d transition intensity while maintaining similar Cu−S covalency as evidenced by similarities between constructs in total LMCT extinction coefficients and Cu−S bond distance as determined by EXAFS. This possibility will require further investigation.

Cu−O distances as determined by EXAFS are consistent with a model in which the relatively strong Glu−Cu bond within the parent Cu(II)GRα_3DChC2 (1.96 Å) is replaced with a much weaker Cu−O/N bond when E41 is mutated to allow water access (e.g., E41A). The differing effects of E41D and E41Q are likely due to the Cu ion positioning required when decreasing the length of the ligating Glu by a methyl group to Asp compared to a more structurally equivalent E41Q mutation. Given the drastic changes in the Cu(II) signal's half-life within Cu(II)-GRα_3DChC2 E41Q and Cu(II)GRα_3DChC2 E41A compared to Cu(II)GRα_3DChC2 and Cu(II)GRα_3DChC2 E41D, it is likely that, while Glu and Asp are able to directly interact, albeit Asp more weakly, Gln or Ala mutations replace this carboxylate interaction with an exogenous water molecule, resulting in a more rapid loss of Cu(II) signal.

X-ray absorption spectra of Cu(I) adducts of GRα_3DChC2, GRα_3DChC2 E41Q, GRα_3DChC2 E41A, and GRα_3DChC2 E41D were measured to examine the effects of these mutations on Cu(I) binding geometry. Grouped together, the XANES analyses of these constructs as well as Cu(I)α_3DChC2 indicate a coordination number between 2 and 3, though our analysis favors 2-coordinate, as detailed previously. While no evidence was found for a direct E41−Cu(I) interaction within EXAFS analysis, it is interesting to note that E41 mutation still has an effect, albeit arguably slight, on Cu(I) geometry, with E41Q measured bond distances on average being longer, and thus more 3-coordinate, while E41A indicates the opposite. These observations argue for a less direct role of E41 in the Cu(I) form of these constructs, with second-sphere effects accounting for shifts in coordination number.

Our interpretation of these data is that the E41 residue of the original CuGRα_3DChC2 interacts with the Cu(II) form of the construct but not the Cu(I) form. E41 mutation to Ala, Gln, or Asp can be used to shift the geometry of the bound Cu(II) and, by doing so, compress or expand hyperfine coupling.

Comparison of reduction/oxidation potentials across the E41 variant series shows that E41 mutations generally have the effect of decreasing the redox potential. It is surprising that E41A and E41Q mutations both have less of an effect on redox potential than E41D, as one would expect the apparently more disruptive E41A and E41Q mutations to have larger effects on Cu(I/II) affinities and thus redox potential. All of these *de novo* constructs are still much higher in redox potential than the native nitrosocyanin's 85 mV, and future work may focus on trying to find means of decreasing E^0. From a design aspect, however, it is useful to know that mutations of E41 allow for vastly different spectroscopic parameters while maintaining similar E^0.

CONCLUSION

Through structural comparison, we have shown the utility of duplicating "heptads" within an α-helical bundle to increase its free energy of unfolding and, therefore, its amenability to more-complex mutation. That such a simple strategy was successful is an indicator of the power of this "inside-out" approach, in which the loop regions of the bundle remain intact while the α-helical region is lengthened. Our laboratory has adapted this strategy to a number of different applications within α-helical bundles, and the new GRANDα_3D (GRα_3D) scaffold's increased free energy of unfolding is being exploited to create more-complex metalloprotein mimics.

Recapitulation of our previously described cupredoxin mimic α_3DChC2 within this new scaffold has proven that the nitrosocyanin-like properties of α_3DChC2 were unrelated to the apo peptide's low free energy of unfolding, as had been previously postulated.[1] Instead, analysis of models based on our X-ray structure suggested that a dissymmetrically oriented copper ion was located within the hydrophobic core of GRα_3DChC2 and that this allowed surface residues access to the metal. We have shown through extensive site-directed mutation studies that a previously unconsidered amino acid designed as part of a salt bridge (glutamate 41) is imperative for Cu(II)GRα_3DChC2's nitrosocyanin-like spectroscopy. Mutation of this amino acid can tune the hyperfine coupling from 160 × 10^{-4} cm^{-1} down to 127 × 10^4 cm^1, shift the σ LMCT transitions from 26 010 to 25 000 cm^{-1}, and alter the ratio of the electronic absorption band intensities ($\varepsilon_{\sigma/\pi}$) from 5.7 to 2.2. Previous nitrosocyanin mimics have been observed within cupredoxin folds, but this construct illustrates that, by accommodating carboxylate interactions, nitrosocyanin's spectroscopic properties can be mimicked within an α-helical structure. Our improved understanding of this *de novo* metalloprotein is an important step in work to control the electronic properties of Cu(II) within an α-helical bundle. We have initiated studies to tune the bound Cu(II) from a red copper site to a green or blue copper site utilizing this new understanding.

Finally, given the difficulty of mutating and expressing nitrosocyanin itself, this study is the first look into how site-directed mutagenesis of a red copper protein would affect the bound copper's electronic and structural properties. Further exploration of these constructs will give a unique angle on the causes of nitrosocyanin's spectroscopic properties that are currently difficult or impossible to study with the native protein.

ASSOCIATED CONTENT

Supporting Information

Table S1, DNA sequences of all genes used during this study; Table S2, native cupredoxins ligand bond distances; Figure S1 and Table S3, comparison of the hydrophobic packing of α_3D, α_3DIV, and GRα_3D; Table

DOI: 10.1021/acs.inorgchem.8b01989
Inorg. Chem. 2018, 57, 12291−12302

S4, spectroscopic parameters of native and *de novo* cupredoxins; Tables S5 and S6 and Figures S2 and S3, Cu(I) or Cu(II) EXAFS fitting parameters; Figures S4 and S5, Cu(I) and Cu(II) XANES analysis figures; Figure S6 and Table S7, MCD analysis of GRα_3DChC2 and GRα_3DChC2 E41D; Figure S7, electrochemical analysis; and Figure S8, EPR spectra and fits (PDF)

AUTHOR INFORMATION

Corresponding Author

*E-mail: vlpec@umich.edu.

ORCID

Aniruddha Deb: 0000-0002-0331-9709
Nicolai Lehnert: 0000-0002-5221-5498
Clotilde Policar: 0000-0003-0255-1650
Cédric Tard: 0000-0002-1515-1915
James E. Penner-Hahn: 0000-0003-0314-1274
Vincent L. Pecoraro: 0000-0002-1540-5735

Notes

The authors declare no competing financial interest.

ACKNOWLEDGMENTS

V.L.P. thanks the U.S. National Institutes of Health (NIH) for financial support of this research (ES012236). The ENS Paris Saclay is acknowledged for E.M.'s Ph.D. fellowship. The FrenchBIC (http://frenchbic.cnrs.fr/) is acknowledged for E.M.'s fellowship that partly funded her stay at V.L.P.'s laboratory. The authors thank Dr. Tyler Pinter for helpful comments and discussion. Use of the Stanford Synchrotron Radiation Lightsource, SLAC National Accelerator Laboratory, is supported by the U.S. Department of Energy (DOE), Office of Science, Office of Basic Energy Sciences under Contract No. DE-AC02-76SF00515. The SSRL Structural Molecular Biology Program is supported by the DOE Office of Biological and Environmental Research, and by the NIH, National Institute of General Medical Sciences (including P41GM103393). The contents of this publication are solely the responsibility of the authors and do not necessarily represent the official views of NIGMS or NIH. This research used resources of the Advanced Photon Source, a U.S. Department of Energy (DOE) Office of Science User Facility operated for the DOE Office of Science by Argonne National Laboratory under Contract No. DE-AC02-06CH11357. Use of the LS-CAT Sector 21 was supported by the Michigan Economic Development Corporation and the Michigan Technology Tri-Corridor (Grant 085P1000817).

REFERENCES

(1) Plegaria, J. S.; Duca, M.; Tard, C.; Friedlander, T. J.; Deb, A.; Penner-Hahn, J. E.; Pecoraro, V. L. De Novo Design and Characterization of Copper Metallopeptides Inspired by Native Cupredoxins. *Inorg. Chem.* **2015**, *54* (19), 9470−9482.

(2) Gray, H. B. Centenary Lecture. Long-range electron-transfer in blue copper proteins. *Chem. Soc. Rev.* **1986**, *15* (1), 17−30.

(3) Gray, H. B.; Malmström, B. G.; Williams, R. J. P. Copper coordination in blue proteins. *JBIC, J. Biol. Inorg. Chem.* **2000**, *5* (5), 551−559.

(4) Solomon, E. I. Spectroscopic Methods in Bioinorganic Chemistry: Blue to Green to Red Copper Sites. *Inorg. Chem.* **2006**, *45* (20), 8012−8025.

(5) Colman, P. M.; Freeman, H. C.; Guss, J. M.; Murata, M.; Norris, V. A.; Ramshaw, J. A. M.; Venkatappa, M. P. X-ray crystal structure analysis of plastocyanin at 2.7 [angst] resolution. *Nature* **1978**, *272* (5651), 319−324.

(6) Penfield, K. W.; Gay, R. R.; Himmelwright, R. S.; Eickman, N. C.; Norris, V. A.; Freeman, H. C.; Solomon, E. I. Spectroscopic studies on plastocyanin single crystals: a detailed electronic structure determination of the blue copper active site. *J. Am. Chem. Soc.* **1981**, *103* (15), 4382−4388.

(7) Gewirth, A. A.; Solomon, E. I. Electronic structure of plastocyanin: excited state spectral features. *J. Am. Chem. Soc.* **1988**, *110* (12), 3811−3819.

(8) LaCroix, L. B.; Shadle, S. E.; Wang, Y.; Averill, B. A.; Hedman, B.; Hodgson, K. O.; Solomon, E. I. Electronic Structure of the Perturbed Blue Copper Site in Nitrite Reductase: Spectroscopic Properties, Bonding, and Implications for the Entatic/Rack State. *J. Am. Chem. Soc.* **1996**, *118* (33), 7755−7768.

(9) Olesen, K.; Veselov, A.; Zhao, Y.; Wang, Y.; Danner, B.; Scholes, C. P.; Shapleigh, J. P. Spectroscopic, Kinetic, and Electrochemical Characterization of Heterologously Expressed Wild-Type and Mutant Forms of Copper-Containing Nitrite Reductase from Rhodobacter sphaeroides 2.4.3. *Biochemistry* **1998**, *37* (17), 6086−6094.

(10) Roger, M.; Biaso, F.; Castelle, C. J.; Bauzan, M.; Chaspoul, F.; Lojou, E.; Sciara, G.; Caffarri, S.; Giudici-Orticoni, M.-T.; Ilbert, M. Spectroscopic Characterization of a Green Copper Site in a Single-Domain Cupredoxin. *PLoS One* **2014**, *9* (6), e98941.

(11) King, J. D.; Harrington, L.; Lada, B. M.; He, G.; Cooley, J. W.; Blankenship, R. E. Site-directed mutagenesis of the highly perturbed copper site of auracyanin D. *Arch. Biochem. Biophys.* **2014**, *564*, 237−243.

(12) Arciero, D. M.; Pierce, B. S.; Hendrich, M. P.; Hooper, A. B. Nitrosocyanin, a Red Cupredoxin-like Protein from Nitrosomonas europaea. *Biochemistry* **2002**, *41* (6), 1703−1709.

(13) Slutter, C. E.; Sanders, D.; Wittung, P.; Malmström, B. G.; Aasa, R.; Richards, J. H.; Gray, H. B.; Fee, J. A. Water-Soluble, Recombinant CuA-Domain of the Cytochrome ba3 Subunit II from Thermus thermophilus. *Biochemistry* **1996**, *35* (11), 3387−3395.

(14) Wittung-Stafshede, P.; Hill, M. G.; Gomez, E.; Di Bilio, A. J.; Karlsson, B. G.; Leckner, J.; Winkler, J. R.; Gray, H. B.; Malmström, B. G. Reduction potentials of blue and purple copper proteins in their unfolded states: a closer look at rack-induced coordination. *JBIC, J. Biol. Inorg. Chem.* **1998**, *3* (4), 367−370.

(15) Randall, D. W.; Gamelin, D. R.; LaCroix, L. B.; Solomon, E. I. Electronic structure contributions to electron transfer in blue Cu and CuA. *JBIC, J. Biol. Inorg. Chem.* **2000**, *5* (1), 16−29.

(16) Savelieff, M. G.; Wilson, T. D.; Elias, Y.; Nilges, M. J.; Garner, D. K.; Lu, Y. Experimental evidence for a link among cupredoxins: Red, blue, and purple copper transformations in nitrous oxide reductase. *Proc. Natl. Acad. Sci. U. S. A.* **2008**, *105* (23), 7919−7924.

(17) Solomon, E. I.; Szilagyi, R. K.; DeBeer George, S.; Basumallick, L. Electronic Structures of Metal Sites in Proteins and Models: Contributions to Function in Blue Copper Proteins. *Chem. Rev.* **2004**, *104* (2), 419−458.

(18) Solomon, E. I.; Hadt, R. G. , Recent advances in understanding blue copper proteins. *Coord. Chem. Rev.* **2011**, *255* (7−8), 774−789.

(19) Lu, Y.; LaCroix, L. B.; Lowery, M. D.; Solomon, E. I.; Bender, C. J.; Peisach, J.; Roe, J. A.; Gralla, E. B.; Valentine, J. S. Construction of a blue copper site at the native zinc site of yeast copper-zinc superoxide dismutase. *J. Am. Chem. Soc.* **1993**, *115* (14), 5907−5918.

(20) Clark, K. M.; Yu, Y.; Marshall, N. M.; Sieracki, N. A.; Nilges, M. J.; Blackburn, N. J.; van der Donk, W. A.; Lu, Y. Transforming a Blue Copper into a Red Copper Protein: Engineering Cysteine and Homocysteine into the Axial Position of Azurin Using Site-Directed Mutagenesis and Expressed Protein Ligation. *J. Am. Chem. Soc.* **2010**, *132* (29), 10093−10101.

(21) Basumallick, L.; Sarangi, R.; DeBeer George, S.; Elmore, B.; Hooper, A. B.; Hedman, B.; Hodgson, K. O.; Solomon, E. I. Spectroscopic and Density Functional Studies of the Red Copper Site in Nitrosocyanin: Role of the Protein in Determining Active Site Geometric and Electronic Structure. *J. Am. Chem. Soc.* **2005**, *127* (10), 3531−3544.

(22) Kachalova, G. S.; Shosheva, A. C.; Bourenkov, G. P.; Donchev, A. A.; Dimitrov, M. I.; Bartunik, H. D. Structural comparison of the poplar

plastocyanin isoforms PCa and PCb sheds new light on the role of the copper site geometry in interactions with redox partners in oxygenic photosynthesis. *J. Inorg. Biochem.* **2012**, *115*, 174−181.
(23) Wijma, H. J.; MacPherson, I.; Farver, O.; Tocheva, E. I.; Pecht, I.; Verbeet, M. P.; Murphy, M. E. P.; Canters, G. W. Effect of the Methionine Ligand on the Reorganization Energy of the Type-1 Copper Site of Nitrite Reductase. *J. Am. Chem. Soc.* **2007**, *129* (3), 519−525.
(24) Lieberman, R. L.; Arciero, D. M.; Hooper, A. B.; Rosenzweig, A. C. Crystal structure of a novel red copper protein from Nitrosomonas europaea. *Biochemistry* **2001**, *40* (19), 5674−5681.
(25) Penfield, K. W.; Gewirth, A. A.; Solomon, E. I. Electronic structure and bonding of the blue copper site in plastocyanin. *J. Am. Chem. Soc.* **1985**, *107* (15), 4519−4529.
(26) Lu, Y.; Berry, S. M.; Pfister, T. D. Engineering Novel Metalloproteins: Design of Metal-Binding Sites into Native Protein Scaffolds. *Chem. Rev.* **2001**, *101* (10), 3047−3080.
(27) Ghosh, D.; Pecoraro, V. L. Understanding Metalloprotein Folding Using a de Novo Design Strategy. *Inorg. Chem.* **2004**, *43* (25), 7902−7915.
(28) Lu, Y.; Yeung, N.; Sieracki, N.; Marshall, N. M. Design of Functional Metalloproteins. *Nature* **2009**, *460* (7257), 855−862.
(29) Zastrow, M. L.; Pecoraro, V. L. , Designing functional metalloproteins: From structural to catalytic metal sites. *Coord. Chem. Rev.* **2013**, *257* (17−18), 2565−2588.
(30) Hu, C.; Chan, S. I.; Sawyer, E. B.; Yu, Y.; Wang, J. Metalloprotein design using genetic code expansion. *Chem. Soc. Rev.* **2014**, *43* (18), 6498−6510.
(31) Yu, F.; Cangelosi, V. M.; Zastrow, M. L.; Tegoni, M.; Plegaria, J. S.; Tebo, A. G.; Mocny, C. S.; Ruckthong, L.; Qayyum, H.; Pecoraro, V. L. Protein Design: Toward Functional Metalloenzymes. *Chem. Rev.* **2014**, *114* (7), 3495−3578.
(32) Holm, R. H.; Kennepohl, P.; Solomon, E. I. Structural and Functional Aspects of Metal Sites in Biology. *Chem. Rev.* **1996**, *96* (7), 2239−2314.
(33) Clark, K. M.; Tian, S.; van der Donk, W. A.; Lu, Y. Probing the role of the backbone carbonyl interaction with the CuA center in azurin by replacing the peptide bond with an ester linkage. *Chem. Commun.* **2017**, *53* (1), 224−227.
(34) Yu, Y.; Petrik, I. D.; Chacón, K. N.; Hosseinzadeh, P.; Chen, H.; Blackburn, N. J.; Lu, Y. Effect of circular permutation on the structure and function of type 1 blue copper center in azurin. *Protein Sci.* **2017**, *26* (2), 218−226.
(35) Tian, S.; Liu, J.; Cowley, R. E.; Hosseinzadeh, P.; Marshall, N. M.; Yu, Y.; Robinson, H.; Nilges, M. J.; Blackburn, N. J.; Solomon, E. I.; Lu, Y. Reversible S-nitrosylation in an engineered azurin. *Nat. Chem.* **2016**, *8*, 670−677.
(36) Shiga, D.; Nakane, D.; Inomata, T.; Funahashi, Y.; Masuda, H.; Kikuchi, A.; Oda, M.; Noda, M.; Uchiyama, S.; Fukui, K.; Kanaori, K.; Tajima, K.; Takano, Y.; Nakamura, H.; Tanaka, T. Creation of a Type 1 Blue Copper Site within a de Novo Coiled-Coil Protein Scaffold. *J. Am. Chem. Soc.* **2010**, *132* (51), 18191−18198.
(37) Shiga, D.; Hamano, Y.; Kamei, M.; Funahashi, Y.; Masuda, H.; Sakaguchi, M.; Ogura, T.; Tanaka, T. Tuning the geometries of a de novo blue copper protein by axial interactions. *JBIC, J. Biol. Inorg. Chem.* **2012**, *17* (7), 1025−1031.
(38) Shiga, D.; Funahashi, Y.; Masuda, H.; Kikuchi, A.; Noda, M.; Uchiyama, S.; Fukui, K.; Kanaori, K.; Tajima, K.; Takano, Y.; Nakamura, H.; Kamei, M.; Tanaka, T. Creation of a Binuclear Purple Copper Site within a de Novo Coiled-Coil Protein. *Biochemistry* **2012**, *51* (40), 7901−7907.
(39) Mann, S. I.; Heinisch, T.; Weitz, A. C.; Hendrich, M. P.; Ward, T. R.; Borovik, A. S. Modular Artificial Cupredoxins. *J. Am. Chem. Soc.* **2016**, *138* (29), 9073−9076.
(40) Bryson, J. W.; Desjarlais, J. R.; Handel, T. M.; Degrado, W. F. From coiled coils to small globular proteins: Design of a native-like three-helix bundle. *Protein Sci.* **1998**, *7* (6), 1404−1414.
(41) Walsh, S. T. R.; Cheng, H.; Bryson, J. W.; Roder, H.; DeGrado, W. F. Solution structure and dynamics of a de novo designed three-helix bundle protein. *Proc. Natl. Acad. Sci. U. S. A.* **1999**, *96* (10), 5486−5491.
(42) Chakraborty, S.; Kravitz, J. Y.; Thulstrup, P. W.; Hemmingsen, L.; DeGrado, W. F.; Pecoraro, V. L. Realization of a Designed Three-Helix Bundle Capable of Binding Heavy Metals in a Tris(Cysteine) Environment. *Angew. Chem., Int. Ed.* **2011**, *50* (9), 2049−2053.
(43) Tebo, A. G.; Hemmingsen, L.; Pecoraro, V. L. Variable primary coordination environments of Cd(II) binding to three helix bundles provide a pathway for rapid metal exchange(). *Metallomics: integrated biometal science* **2015**, *7* (12), 1555−1561.
(44) Tebo, A. G.; Pinter, T. B. J.; García-Serres, R.; Speelman, A. L.; Tard, C.; Sénéque, O.; Blondin, G.; Latour, J.-M.; Penner-Hahn, J.; Lehnert, N.; Pecoraro, V. L. Development of a Rubredoxin-Type Center Embedded in a *de Novo*-Designed Three-Helix Bundle. *Biochemistry* **2018**, *57* (16), 2308−2316.
(45) Plegaria, J. S.; Dzul, S. P.; Zuiderweg, E. R. P.; Stemmler, T. L.; Pecoraro, V. L. Apoprotein Structure and Metal Binding Characterization of a de Novo Designed Peptide, α3DIV, that Sequesters Toxic Heavy Metals. *Biochemistry* **2015**, *54* (18), 2858−2873.
(46) Farrer, B. T.; Harris, N. P.; Balchus, K. E.; Pecoraro, V. L. Thermodynamic Model for the Stabilization of Trigonal Thiolato Mercury(II) in Designed Three-Stranded Coiled Coils. *Biochemistry* **2001**, *40* (48), 14696−14705.
(47) Su, J. Y.; Hodges, R. S.; Kay, C. M. Effect of Chain Length on the Formation and Stability of Synthetic α-Helical Coiled Coils. *Biochemistry* **1994**, *33* (51), 15501−15510.
(48) Kim, D. E.; Chivian, D.; Baker, D. Protein structure prediction and analysis using the Robetta server. *Nucleic Acids Res.* **2004**, *32*, W526−W531.
(49) Raman, S.; Vernon, R.; Thompson, J.; Tyka, M.; Sadreyev, R.; Pei, J.; Kim, D.; Kellogg, E.; DiMaio, F.; Lange, O.; Kinch, L.; Sheffler, W.; Kim, B.-H.; Das, R.; Grishin, N. V.; Baker, D. Structure prediction for CASP8 with all-atom refinement using Rosetta. *Proteins: Struct., Funct., Genet.* **2009**, *77* (S9), 89−99.
(50) Song, Y.; DiMaio, F.; Wang, R. Y.-R.; Kim, D.; Miles, C.; Brunette, T. J.; Thompson, J.; Baker, D. High-Resolution Comparative Modeling with RosettaCM. *Structure* **2013**, *21* (10), 1735−1742.
(51) Plegaria, J. S.; Pecoraro, V. L. Sculpting Metal-binding Environments in De Novo Designed Three-helix Bundles. *Isr. J. Chem.* **2015**, *55* (1), 85−95.
(52) Paulat, F.; Lehnert, N. Detailed Assignment of the Magnetic Circular Dichroism and UV−vis Spectra of Five-Coordinate High-Spin Ferric [Fe(TPP)(Cl)]. *Inorg. Chem.* **2008**, *47* (11), 4963−4976.
(53) Otwinowski, Z.; Minor, W. Processing of X-ray diffraction data collected in oscillation mode. *Methods in Enzymology*, Vol. *276*; Academic Press, 1997; pp 307−326.
(54) Terwilliger, T. C.; Adams, P. D.; Read, R. J.; McCoy, A. J.; Moriarty, N. W.; Grosse-Kunstleve, R. W.; Afonine, P. V.; Zwart, P. H.; Hung, L.-W. Decision-making in structure solution using Bayesian estimates of map quality: the PHENIX AutoSol wizard. *Acta Crystallogr., Sect. D: Biol. Crystallogr.* **2009**, *65* (6), 582−601.
(55) McCoy, A. J.; Storoni, L. C.; Read, R. J. Simple algorithm for a maximum-likelihood SAD function. *Acta Crystallogr., Sect. D: Biol. Crystallogr.* **2004**, *60* (7), 1220−1228.
(56) Vagin, A.; Teplyakov, A. Molecular replacement with MOLREP. *Acta Crystallogr., Sect. D: Biol. Crystallogr.* **2010**, *66* (1), 22−25.
(57) Potterton, E.; Briggs, P.; Turkenburg, M.; Dodson, E. A graphical user interface to the CCP4 program suite. *Acta Crystallogr., Sect. D: Biol. Crystallogr.* **2003**, *59* (7), 1131−1137.
(58) Winn, M. D.; Ballard, C. C.; Cowtan, K. D.; Dodson, E. J.; Emsley, P.; Evans, P. R.; Keegan, R. M.; Krissinel, E. B.; Leslie, A. G. W.; McCoy, A.; McNicholas, S. J.; Murshudov, G. N.; Pannu, N. S.; Potterton, E. A.; Powell, H. R.; Read, R. J.; Vagin, A.; Wilson, K. S. Overview of the CCP4 suite and current developments. *Acta Crystallogr., Sect. D: Biol. Crystallogr.* **2011**, *67* (4), 235−242.
(59) McCoy, A. J.; Grosse-Kunstleve, R. W.; Adams, P. D.; Winn, M. D.; Storoni, L. C.; Read, R. J. Phaser crystallographic software. *J. Appl. Crystallogr.* **2007**, *40* (4), 658−674.

(60) Plegaria, J. S.; Pecoraro, V. L. De Novo Design of Metalloproteins and Metalloenzymes in a Three-Helix Bundle. In *Computational Design of Ligand Binding Proteins*; Stoddard, B. L., Ed.; Springer: New York, 2016; pp 187−196.
(61) Hirel, P. H.; Schmitter, M. J.; Dessen, P.; Fayat, G.; Blanquet, S. Extent of N-terminal methionine excision from Escherichia coli proteins is governed by the side-chain length of the penultimate amino acid. *Proc. Natl. Acad. Sci. U. S. A.* **1989**, *86* (21), 8247−8251.
(62) Emsley, P.; Cowtan, K. Coot: model-building tools for molecular graphics. *Acta Crystallogr., Sect. D: Biol. Crystallogr.* **2004**, *60* (12), 2126−2132.
(63) Bricogne, G.; Blanc, E.; Brandl, M.; Flensburg, C.; Keller, P.; Paciorek, W.; Roversi, P., Smart, O. S., Vonrhein, C.; Womack, T. O. *BUSTER*, version 2.10.2; Global Phasing Ltd.: Cambridge, UK 2016.
(64) Chen, V. B.; Arendall, W. B., III; Headd, J. J.; Keedy, D. A.; Immormino, R. M.; Kapral, G. J.; Murray, L. W.; Richardson, J. S.; Richardson, D. C. MolProbity: all-atom structure validation for macromolecular crystallography. *Acta Crystallogr., Sect. D: Biol. Crystallogr.* **2010**, *66* (1), 12−21.
(65) Kleywegt, G. J.; Harris, M. R.; Zou, J.-y.; Taylor, T. C.; Wahlby, A.; Jones, T. A. The Uppsala Electron-Density Server. *Acta Crystallogr., Sect. D: Biol. Crystallogr.* **2004**, *60* (12), 2240−2249.
(66) George, G. N.; Pickering, I. J. EXAFSPAK, http://www-ssrl.slac.stanford.edu/exafspak.html.
(67) Ankudinov, A. L.; Rehr, J. J. Relativistic calculations of spin-dependent x-ray-absorption spectra. *Phys. Rev. B: Condens. Matter Mater. Phys.* **1997**, *56* (4), R1712−R1716.
(68) Weng, T.-C.; Waldo, G. S.; Penner-Hahn, J. E. A method for normalization of X-ray absorption spectra. *J. Synchrotron Radiat.* **2005**, *12* (4), 506−510.
(69) Krivov, G. G.; Shapovalov, M. V.; Dunbrack, R. L. Improved prediction of protein side-chain conformations with SCWRL4. *Proteins: Struct., Funct., Genet.* **2009**, *77* (4), 778−795.
(70) Willard, L.; Ranjan, A.; Zhang, H.; Monzavi, H.; Boyko, R. F.; Sykes, B. D.; Wishart, D. S. VADAR: a web server for quantitative evaluation of protein structure quality. *Nucleic Acids Res.* **2003**, *31* (13), 3316−3319.
(71) Chen, C. R.; Makhatadze, G. I. ProteinVolume: calculating molecular van der Waals and void volumes in proteins. *BMC Bioinf.* **2015**, *16* (1), 101.
(72) Carra, J. H.; Privalov, P. L. Thermodynamics of denaturation of staphylococcal nuclease mutants: an intermediate state in protein folding. *FASEB J.* **1996**, *10* (1), 67−74.
(73) Santoro, M. M.; Bolen, D. W. Unfolding free energy changes determined by the linear extrapolation method. 1. Unfolding of phenylmethanesulfonyl.alpha.-chymotrypsin using different denaturants. *Biochemistry* **1988**, *27* (21), 8063−8068.
(74) Kau, L. S.; Spira-Solomon, D. J.; Penner-Hahn, J. E.; Hodgson, K. O.; Solomon, E. I. X-ray absorption edge determination of the oxidation state and coordination number of copper. Application to the type 3 site in Rhus vernicifera laccase and its reaction with oxygen. *J. Am. Chem. Soc.* **1987**, *109* (21), 6433−6442.
(75) Siluvai, G. S.; Mayfield, M.; Nilges, M. J.; DeBeer George, S.; Blackburn, N. J. Anatomy of a Red Copper Center: Spectroscopic Identification and Reactivity of the Copper Centers of Bacillus subtilis Sco and Its Cys-to-Ala Variants. *J. Am. Chem. Soc.* **2010**, *132* (14), 5215−5226.
(76) Hahn, J. E.; Scott, R. A.; Hodgson, K. O.; Doniach, S.; Desjardins, S. R.; Solomon, E. I. Observation of an electric quadrupole transition in the X-ray absorption spectrum of a Cu(II) complex. *Chem. Phys. Lett.* **1982**, *88* (6), 595−598.
(77) de Groot, F.; Vanko, G.; Glatzel, P. The 1s x-ray absorption pre-edge structures in transition metal oxides. *J. Phys.: Condens. Matter* **2009**, *21* (10), 104207.
(78) Ghosh, S.; Xie, X.; Dey, A.; Sun, Y.; Scholes, C. P.; Solomon, E. I. Thermodynamic equilibrium between blue and green copper sites and the role of the protein in controlling function. *Proc. Natl. Acad. Sci. U. S. A.* **2009**, *106* (13), 4969−4974.
(79) Ruckthong, L.; Stuckey, J. A.; Pecoraro, V. L. Methods for Solving Highly Symmetric de Novo Designed Metalloproteins: Crystallographic Examination of a Novel Three Stranded Coiled Coil structure containing D-amino Acids. *Methods Enzymol.* **2016**, *580*, 135−148.
(80) Bennett, B.; Kowalski, J. M. EPR Methods for Biological Cu(II): L-Band CW and NARS. In *Methods in Enzymology*, Vol. *563*; Qin, P. Z., Warncke, K., Eds.; Academic Press: 2015; Chapter 13, pp 341−361.
(81) Peisach, J.; Blumberg, W. E. Structural implications derived from the analysis of electron paramagnetic resonance spectra of natural and artificial copper proteins. *Arch. Biochem. Biophys.* **1974**, *165* (2), 691−708.
(82) Goodman, B. A.; Raynor, J. B. Electron Spin Resonance of Transition Metal Complexes. In *Advances in Inorganic Chemistry and Radiochemistry*, Vol. *13*; Emeléus, H. J., Sharpe, A. G., Eds.; Academic Press: 1970; pp 135−362.
(83) Sharnoff, M. Electron Paramagnetic Resonance and the Primarily 3d Wavefunctions of the Tetrachlorocuprate Ion. *J. Chem. Phys.* **1965**, *42* (10), 3383−3395.
(84) Solomon, E. I.; Hare, J. W.; Gray, H. B. Spectroscopic studies and a structural model for blue copper centers in proteins. *Proc. Natl. Acad. Sci. U. S. A.* **1976**, *73* (5), 1389−1393.
(85) Solomon, E. I.; Hare, J. W.; Dooley, D. M.; Dawson, J. H.; Stephens, P. J.; Gray, H. B. Spectroscopic studies of stellacyanin, plastocyanin, and azurin. Electronic structure of the blue copper sites. *J. Am. Chem. Soc.* **1980**, *102* (1), 168−178.
(86) Lancaster, K. M.; George, S. D.; Yokoyama, K.; Richards, J. H.; Gray, H. B. Type-zero copper proteins. *Nat. Chem.* **2009**, *1* (9), 711−715.
(87) Lancaster, K. M.; Farver, O.; Wherland, S.; Crane, E. J.; Richards, J. H.; Pecht, I.; Gray, H. B. Electron Transfer Reactivity of Type Zero Pseudomonas aeruginosa Azurin. *J. Am. Chem. Soc.* **2011**, *133* (13), 4865−4873.
(88) Lancaster, K. M.; Zaballa, M.-E.; Sproules, S.; Sundararajan, M.; DeBeer, S.; Richards, J. H.; Vila, A. J.; Neese, F.; Gray, H. B. Outer-Sphere Contributions to the Electronic Structure of Type Zero Copper Proteins. *J. Am. Chem. Soc.* **2012**, *134* (19), 8241−8253.
(89) Potapov, A.; Lancaster, K. M.; Richards, J. H.; Gray, H. B.; Goldfarb, D. Spin Delocalization Over Type Zero Copper. *Inorg. Chem.* **2012**, *51* (7), 4066−4075.